International Journal of Rock Mechanics & Mining Sciences 127 (2020) 104237

Contents lists available at ScienceDirect

International Journal of Rock Mechanics and Mining Sciences

journal homepage: http://www.elsevier.com/locate/ijrmms

Experimental quantification of vertical stresses during gravity flow in block caving

Raúl Castro [a,b,*], René Gómez [c], Matthew Pierce [d], Juan Canales [b]

[a] Laboratorio de Block Caving, Advanced Mining Technology Center, Universidad de Chile, Chile
[b] Departamento de Ingeniería de Minas, Universidad de Chile, Chile
[c] Facultad de Ingeniería, Universidad de Concepción, Chile
[d] Pierce Engineering, Minnesota, United States

ARTICLE INFO

Keywords:
Caving mining
Granular material
Gravity flow
Induced stresses
Stress
Rock

ABSTRACT

Usually in block and panel caving mines, when the caving connects to the surface, monitoring of vertical stresses over production drifts is minimal due to the low probability of seismic events. However, when the stresses over the production level are related to an overburden by fragmented rock, the draw policies highly influence induced stress. In this context, we present an experimental set up using a laboratory-scale model to identify the role of draw strategy on induced vertical stresses in a block-caving layout. Here, three draw strategies are studied: isolated draw, panel caving draw, and block caving draw. Results show that induced vertical stresses can vary between 0.3 and 2.8 times their initial vertical value and are highly influenced by both the distance from the extraction front and the dimension of draw and non-draw areas. These findings provide useful information to support the system design in block caving or panel caving methods to decrease induced vertical stresses related to draw and define rules of extraction in an effort to avoid problems related to the maximum stress that can be expected on production-level pillars.

1. Introduction

Current challenges in the mining environment include factors such as deeper deposits, harder rock, higher in-situ stresses, greater production demand and increased costs.[1,2] One issue which can have consequences at greater depths is that the rock mass already subjected to high stresses suffers even higher induced stresses during mining activities. In particular, induced stress occurs during the caving propagation stage in the advancing undercut front,[3–5] where damage has been observed and reported in several block caving mines,[6–11] mainly related to drift convergence and pillar failure. Measurements of stresses, strain, crack extension and seismicity have been carried out at this stage.[12–15] However, in caving mines with greater depths, the column height of caved rock also increases, and consequently, there is an overload on the production level. Usually in block or panel caving mines, when the caving propagation connects to surface, vertical stress over the production drifts is not closely monitored because of the low frequency and magnitude of seismic events. Nevertheless, experience indicates that production drift stability can also be affected during ore extraction in productive areas[16–20] causing drift convergence, concrete slabbing at the walls, collapse and closure.

In granular material, such as caved rock ore, vertical stresses are significantly lower than total column weight because of the arching effect generated by shear stresses due to the rock friction. Janssen [21] initially postulated Eq. (1) that provides the mean vertical stress, $\overline{\sigma_{v,0}}$ (Pa) in certain depth, z (m), considering overload, Q_0, [22]

$$\overline{\sigma_{v,0}} = \frac{R_h \rho_b g}{\mu k}\left(1 - e^{-\frac{\mu k z}{R_h}}\right) + Q_0\left(e^{-\frac{\mu k z}{R_h}}\right) \quad (1)$$

Where R_h is the hydraulic radius (area/perimeter; m) introduced by, [23] ρ_b is the bulk density (kg/m^3), g is the gravity constant (m/s^2), k is the friction parameter that represents the horizontal and vertical stress ratio, σ_h/σ_v, z is the depth of caved rock (m), Q_0 is the initial vertical overload (Pa) and μ is the friction between particles and model wall expressed usually by $\tan(\varphi_w)$, where φ_w is the friction angle of bin walls (degrees). This equation gives a reasonable result in static conditions. However, one of the common problems is determining the k parameter because of the high variability of stress in granular material. Different

* Corresponding author. Laboratorio de Block Caving, Advanced Mining Technology Center, Universidad de Chile, Chile.
E-mail address: rcastro@ing.uchile.cl (R. Castro).

https://doi.org/10.1016/j.ijrmms.2020.104237
Received 13 March 2019; Received in revised form 29 January 2020; Accepted 30 January 2020
Available online 5 February 2020

approaches have been used to define k such as, [24]

$$k = 1 - sen(\varphi) \tag{2}$$

Where φ is the material internal friction angle, the relation $\varphi > \varphi_w$ has been reported.[23–25] Other approaches to define k are presented in Eqs. (3) and (4),

$$k = \frac{1 - sen(\varphi)}{1 + sen(\varphi)} \tag{3}$$

Eq. (3) is defined as an Active case, when $\sigma_h < \sigma_v$ and Eq. (4) is defined as a Passive case, when $\sigma_h > \sigma_v$ [26]

$$k = \frac{1 + sen(\varphi)}{1 - sen(\varphi)} \tag{4}$$

Walker [22] introduces in Eq. (5) a general relation for k using the Mohr-Coulomb circle considering that horizontal and vertical stresses are not necessarily the principal stresses.

$$k = \frac{1 - sen^2(\varphi)}{1 + sen^2(\varphi)} \tag{5}$$

The equations above were developed in physical models to quantify the magnitudes and distribution of stresses in static and dynamic conditions.[21–31] Eqs. (2), (3) and (5) have shown good correlation under static conditions. In dynamic conditions, different results have been reported for k and μ parameters in physical and numerical models, [24,32–34] mainly as a function of the granular material's height. However, granular materials used in these studies (e.g. bean, corn, sand, wheat, barley and coke) are different from material found in the mining environment, where wide particle size distributions, high strength, major internal friction angles and angular fragment shapes are common. Few physical models emulating mining conditions have been developed.[35–37]

When granular material is under flow, at least two main zones – the movement zone and the stagnant zone – can be identified. In the movement zone (or draw zone), porosity increases and vertical stresses decrease due to flow, while in the stagnant zone (or non-draw zone) vertical stresses increase. Experimental measures have shown that stresses can be transferred from the movement zone to the stagnant zone during flow.[35] Then, induced vertical stresses over the production drift depend on the movement of gravity flow zones. In the same way, Lorig [38] postulated that stresses in the isolated movement zone (IMZ) tend to be lower than in surrounding stagnant material. This may occur because stresses are transferred through shear forces acting on boundaries between flow and stagnant material. Furthermore, it was concluded in Ref. 39 that the mean magnitude of forces acting inside the IMZ is independent of the column height and weight.

Pierce [39] proposed applying the tributary area theory to determine the mean vertical stresses in the stagnant zone, $\overline{\sigma}_v^{SZ}$, as:

$$\overline{\sigma}_v^{SZ} = \frac{\overline{\sigma}_{v,0} A_T - \sum_{i=1}^{n} \overline{\sigma}_{v,i}^{MZ} A_i}{A_{sz}} \tag{6}$$

Where $\overline{\sigma}_{v,0}$ is the mean vertical stress before draw (initial condition, Pa), A_T is total area (m^2), $\overline{\sigma}_{v,i}^{MZ}$ is the mean vertical stress of the movement zone i calculated using Eq. (1) and Eq. (3) (Pa), A_i is the area of the movement zone i (m^2) and A_{sz} is the area of the stagnant zone (m^2). Areas are where the caved material is placed in a plan view.

In caving mines, the draw is different in each case. For example, block caving extracts material in a different way than panel caving. Information on the influence of different kinds of draw on induced vertical overloads on the production level is, thus, generally lacking. Then, the objective of this investigation is to use laboratory-scale experiments to quantify the role of draw strategy on induced vertical stresses over pillars located in the production levels to define draw policies that minimize induced stress in critical areas. In particular, nowadays a number of active or planned block and panel caving operations are subjected to greater depths such as El Teniente and Chuquicamata's Underground Project in Chile, the Deep Ore Zone and Deep Mill Level Zone in Indonesia, Resolution Copper and the Henderson mine in the United States and Cadia East in Australia.

2. Experimental methodology

Here a physical model for studying the vertical stress behaviour under flow conditions was constructed representing different draw strategies used in block and panel caving.

2.1. Similitude analysis

The focus of this work is to quantify stresses on granular material for block caving applications using laboratory-scale experiments. For this reason, the geometric similitude is kept constant both in the physical model and the granular material with a length scale factor, λ_l, of 1:200. Furthermore, following conditions of similitude, cohesionless material is used to study stresses on granular material [35] to avoid adhesive forces such as Van der Wall's forces, liquid bridges and electrostatic effect at laboratory scale. Then the material used must be dry and include fragment sizes larger than 0.06 mm.[40] On the other hand, the gravity, bulk density and residual friction angle scale factors are the same in the model as at mine scale, respectively $\lambda_g = \lambda_\rho = \lambda_\varphi = 1$. Then, the scale of stresses is equal to the length scale factor, $\lambda_\sigma = \lambda_l$. This geometrical scale considered (length scale, $\lambda_l = 1/200$) ensures representation of the induced stress phenomena. According to the scaling laws,[35] the similitude's parameters are shown in Table 1. Here physical variables are based on the length scale used.

The following assumptions and simplifications were made to study the stress behaviour in block caving through physical modelling: (1) It is assumed that the rock mass has caved to surface, forces in the system are due to the material's weight, and in-situ stresses are not present. (2) The granular flow occurs in a 3D environment. (3) The rock breakage mechanism related to secondary fragmentation is not considered. (4) The geometries of the flow zones in the physical model are comparable as long as the materials have equal friction angles and particle shapes. The influence of friction in the model's container walls is discussed in section 2.2.

2.2. Physical model

The physical model represents a section of a mine operated by Block or Panel caving with the following dimensions: 140 m length, 46 m width and 480 m column height (see Fig. 1). The scale was chosen to represent a high column height where vertical stress at the bottom would be significant. In the production level, we selected El Teniente's 30 m × 15 m layout.

The mine section corresponds to three production drifts and nine extraction drifts, which represent a total of 36 drawpoints (Fig. 2 and Fig. 3-a). Fig. 2 shows the dimensions of the production level in the physical model. Fine material was glued on the crown pillar over the production drifts to represent the rock friction over pillars and the flow zones' geometries, simulating 3D drawbells.

Table 1
Scale factors based on length scale.

Variable	Factor	Scale factor	Value
Length	λ_L	λ_L	0.005
Area	λ_A	λ_L^2	0.000025
Volume	λ_V	λ_L^3	0.000000125
Time	λ_T	$\lambda_L^{0.5}$	0.0707
Weight	λ_W	λ_L^3	0.000000125
Stress	λ_S	λ_L	0.005
Friction angle	λ_φ	1	1
Density	λ_ρ	1	1

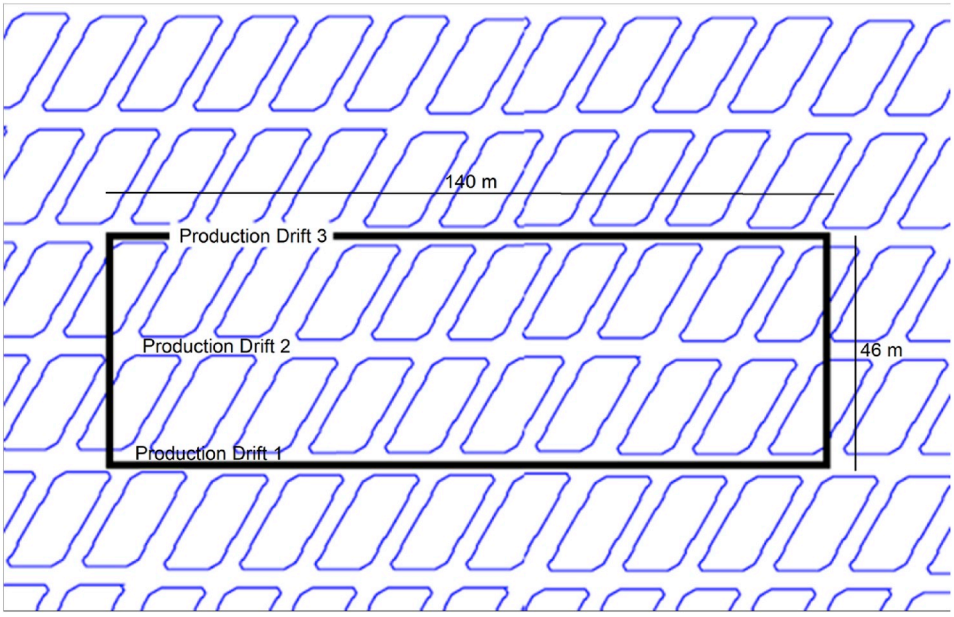

Fig. 1. Mine area represented in the physical model.

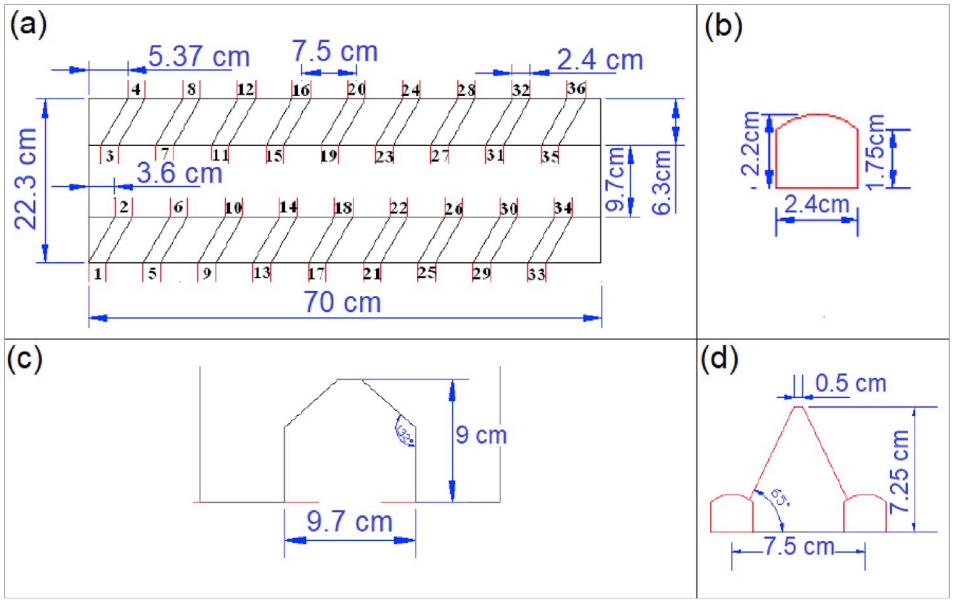

Fig. 2. Geometry of production level represented at the physical model scale.

The walls of the physical model as shown in Fig. 3-b were made of plexiglass. The plexiglass allows movement zones to be observed in the model. This material also increased vertical stress compared with horizontal stress because of the low friction between plexiglass and granular material. For minor frictions, shear forces decrease between the model wall and granular material, then more weight is transferred to the bottom (increasing vertical stress estimated there). For example, we can calculate a vertical stress of 1.35 MPa applying Eq. (1), considering a depth of 500 m, an internal friction angle of 39°, a hydraulic radius of 16.9 m, a bulk density of 1.4 t/m^3 and a wall friction angle of 25°. If we considered a higher friction angle, like the internal friction angle of 39°, a hydraulic radius 74% higher gives us the same vertical stress. For this reason, in this study vertical stress results, σ_v, will be analysed as a function of their initial value, $\sigma_{v,0}$, using the ratio $\sigma_v/\sigma_{v,0}$.

Up to six load cells were located within the model over the crown pillar for vertical stress measurements. Each load cell has a precision of ±0.039 kPa (8 g), a length of 11.5 cm and an area of 20 cm^2. The position of load cells over the crown pillar depends on the purpose of the experiment. Thus, load cell location is shown with the results for each test in Section 3 (Figs. 6, 9, 12 and 15).

2.3. Model media

Tests used crushed sulphide ore with a high aspect ratio (sphericity 0.58 and roundness 0.25, Cho et al.[41] methodology), which is representative of caved rock. The particle size distribution was obtained by scaling (1:200) the primary fragmentation curve expected for Chuquicamata Underground Block caving project (see Fig. 4). The ore characteristics are shown in Table 2.

Sulphide ore corresponds to a biotite and amphibole granitoid, showing metallic mineralization of pyrite, chalcopyrite and bornite. Potasic and propilitic alteration can be seen in the rock samples and

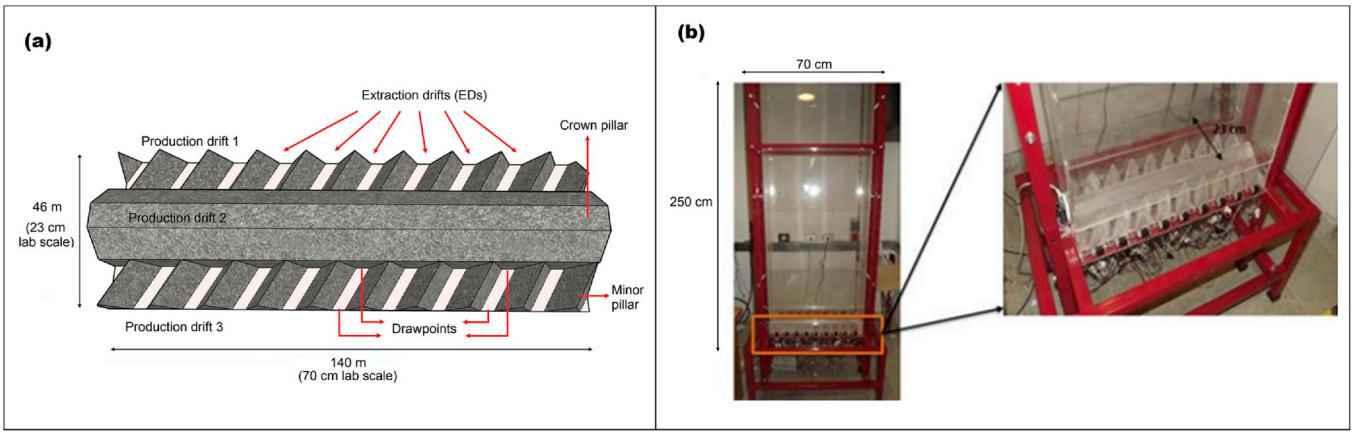

Fig. 3. (a) Sector studied in experiments and main structures, plan view (b) Physical model of plexiglass used in laboratory.

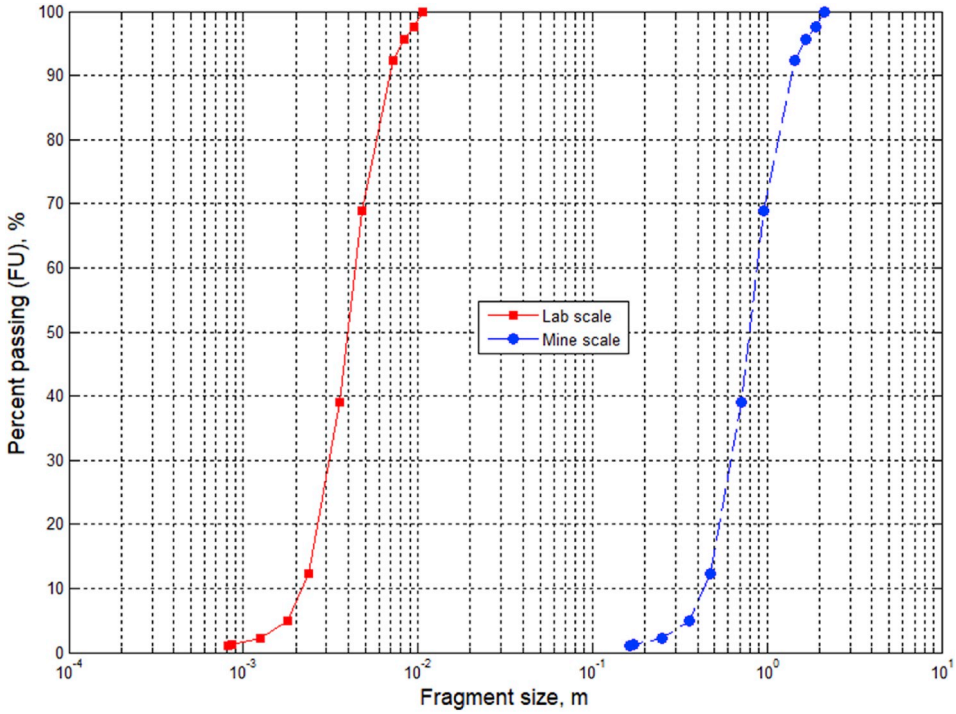

Fig. 4. Fragment size distribution curve used in experiments scaled from a real Block-caving size distribution curve.

Table 2
Ore characterization.

Parameter	Value	Unit
Mean size, d_{50}	4.0	mm
Coefficient of uniformity, Cu	2.0	
Point load index, IS_{50}	6.2 ± 1.6	MPa
Density	2.6	t/m3
Bulk density	1.42	t/m3
Porosity	44	%
Friction angle	39	°
Repose angle	29	°

mafic minerals, respectively.

2.4. Experimental set-up and procedure

The main objective of this work is to study the stresses induced by ore draw, considering common draw practices applied in Block and Panel caving mines. Undercutting development, in Block and Panel caving, is the principal difference between them. Block-caving undercutting is performed in just one stage, or block, at a time (Fig. 5-a), whereas panel-caving undercutting is performed over time by opening drawbells monthly (Fig. 5-b). These differences usually imply that at the beginning of block caving extraction, all drawpoints of one block could be available. However, for different operational reasons, unmoved zones without extraction or overdrawn zones may also exist. On the other hand, in panel caving, it is common to find open drawpoints, closed drawpoints, and drawpoints with differences in their extraction percentage.

Table 3 lists the four experimental set ups with their objectives, as well as the draw strategy and the procedure chosen. To observe and quantify result variability, two tests (A and B) were carried out with each experimental set up (Tests 0, 1, 2 and 3) for a total of 8 experiments. We defined different draw strategies in each test then grouped results according to the draw strategy used for analysing them: isolated draw (base case), panel caving and block caving draw strategies, respectively.

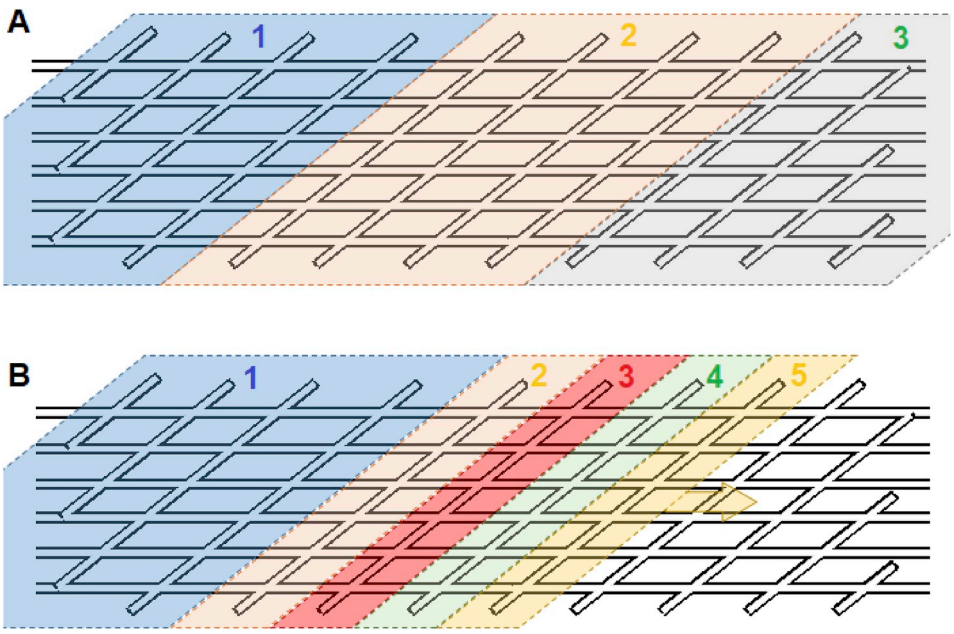

Fig. 5. Plan views (a) Block caving strategy: in blocks 1, 2 and 3 the extraction begins at different periods. Each block should be drawn uniformly. (b) Panel caving strategy: in panels 1, 2, 3, 4 and 5 the extraction begins consecutively. Panels have different extraction percentages; greater percentages are in the first panels.

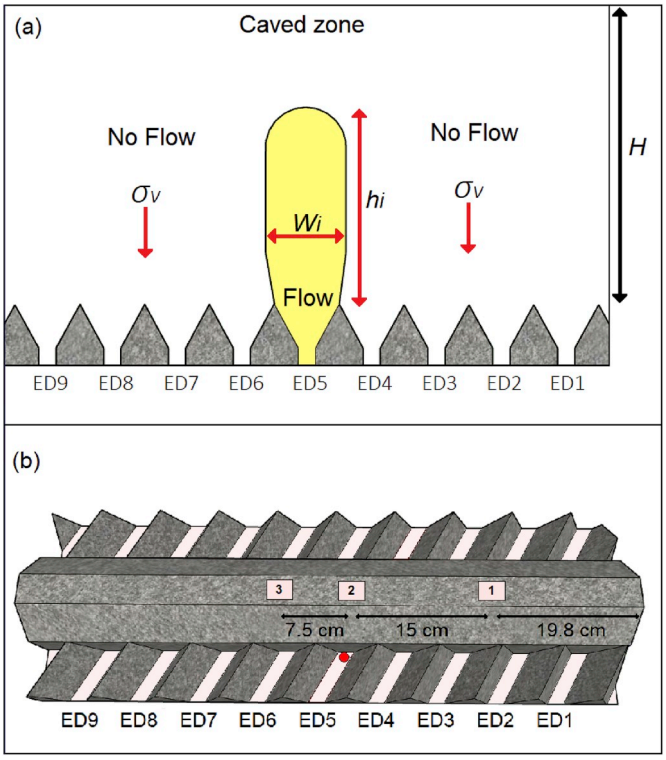

Fig. 6. (a) Isolated draw strategy configuration (front view) and (b) Load cell location over crown pillar.

For each test, the load cells were located based on the point of interest defined by the draw strategy. The material described in the Model Media section, previously homogenised, was then loaded in the physical model to the top (2.5 m). The draw strategy defined for the test was then programed through a servo-assisted motor. In block caving draw strategies, all drawpoints were drawn at the same time until near the end of the tests when active drawpoints were stopped and drawpoints located under the unmoved zone were drawn. For the panel caving draw strategy, the extraction was carried out through a group of extraction drifts continuously until 1 kg per drawpoint was extracted; the drawpoints were then incorporated and/or closed depending on the period of extraction following a panel caving scenario. In this work, the effect of rate of draw was not studied because the stresses measured in the load cells changed almost instantly in all extraction policies observed regardless of extraction velocity.

Table 3
Experimental set-up of gravity flow draw strategies.

Test	Name	Objective	Procedure
0	Isolated draw	To measure IMZ and vertical pressures over the crown pillar for a single drawpoint.	Extraction was carried out from one drawpoint (from Extraction Drift (ED5)) next to the crown pillar. Twenty kilograms of ore drawn at 2.5 kg/h.
1	Panel caving	To measure vertical pressures over the crown pillar considering a panel caving draw scenario.	Extraction was done from ED1 up to ED7. In total, one kg were drawn per drawpoint. During test EDs 1 and 2 were closed and EDs 6 and 7 opened. Test draw rate ~5 kg/h.
2	Block caving – 60 m of unmoved zone	To measure vertical pressures over the crown pillar with an intermediate non-draw area, following a block-caving draw scenario.	ED 1 to 3 and ED 7 to 9 were drawn at the same rate until flow zones reached the surface. Afterwards, extraction was done in ED 4 to 6. Test draw rate ~6.5 kg/h.
3	Block caving – 30 m of unmoved zone	To measure vertical pressures over the crown pillar with a smaller intermediate non-draw area.	Extraction was conducted in all EDs except ED5. At the end of the experiment, extraction was conducted in ED5. Test draw rate ~6.5 kg/h.

2.5. Initial stress conditions

Initial vertical stresses were measured in all tests as the following: 14.8 ± 3.2 kPa in Test 0, 17.8 ± 1.8 kPa in Test 1, 27.7 ± 3.7 kPa in Test

2, 18.3 ± 3.7 kPa in Test 3 and the initial vertical stresses based on Eq. (1) is 18.7 kPa. Here the mean vertical stress is based on the material characteristics defined in Table 2 and assuming $k = 0.37$. The initial vertical stress ranges are expected for physical measurement of granular material due to arching, as reported by other studies.[31,35–37]

3. Draw test results

In this section vertical stress measurements are presented during draw condition. In the first test run, the extraction from one drawpoint defines the IMZ geometry of granular material used. Then, panel and block caving draw strategies are tested showing the influence of the extraction strategy on induced stress.

3.1. Test 0: isolated draw

In this test, ore draws from just one drawpoint located in the middle of the model (see Fig. 6). Fig. 6-b indicates the load cells' location over the crown pillar. The evolution of the IMZ geometry is according to the kinematic theory normalized by d_{50}, $w = 3.42\sqrt{h}$ [42] where w is the IMZ width and h is the IMZ height presented against results in Fig. 7.

During this test, the IMZ radius reached 7.8 cm when 0.7 kg of material were extracted (Fig. 8, right vertical axis). Here, load cells 2 and 3 were below the shadow of the flow zone. Then, the IMZ radius reached 16 cm when 14.6 kg of material were extracted, over load cell 1 (located at 15.8 cm from the active drawpoint).

We observed that vertical stress decreased in load cells closer to the drawpoint under extraction (load cells 2 and 3). Load cell 2 decreased 0.4 times its initial value, whereas load cell 3 decreased its initial value 0.6 times. Load cell 2 is closer than load cell 3 to the drawpoint under extraction; then a distribution of vertical stress into the IMZ can be assumed increasing from the IMZ's centre. It is known that greater (higher) porosity in granular material flow is generated next to the extraction point. In draw zones, the bulk density is decreased due to greater porosity. Greater porosity also implies fewer contact points to transfer stresses in the granular material, which increases the stress transfer on more compacted material, which in this case is the material found in the non-draw zones.

On the other hand, load cell 1 showed no major variation from its initial load condition. It can be seen that inside the IMZ, vertical stress was lower than initial stress, as expected, and decreased closer to the drawpoint. In the non-draw zone, overstress (on load cell 1) was not observed. Possible reasons for this are its proximity to the flow zone, the ratio between the draw and non-draw zones, and/or a shadow effect cast by the IMZ. Further experiments could be done to identify the cause or causes of this effect.

3.2. Test 1: panel caving draw strategy

In test 1, various drawpoints were opened based on the panel caving strategy defined in section 2.4. Extraction drifts were drawn one by one from right to left (Fig. 9-a), in accordance with a common production plan. Experiments here show a mass flow zone (interactive draw between drawpoints under extraction). The extraction drifts (ED) were added from ED1 to ED7, between 27.1 and 47.7 kg ore was drawn from ED1 to ED5, between 47.7 and 67.5 kg ore was drawn from ED3 to ED6, and between 67.5 and 78.2 kg ore was drawn from ED3 to ED7.

Fig. 9-b shows the locations of the six load cells. This distribution allows vertical stress measurements in draw and non-draw zones during extraction. Here, the addition of extraction drifts caused the formation of an unmoved zone in front of the extraction front. Fig. 10 shows the test's evolution, in which the width of the non-draw zone (defined by *Wr*) continuously decreases while new EDs begin extraction. Induced vertical stress in a non-draw zone will necessarily increase if its area is decreased, as observed in Fig. 11.

Fig. 11 illustrates results for all load cells. The stress measurements show overloads in the non-draw zone (also known as stagnant zone) and under-loads in the draw zone (movement zone). Stresses recorded by

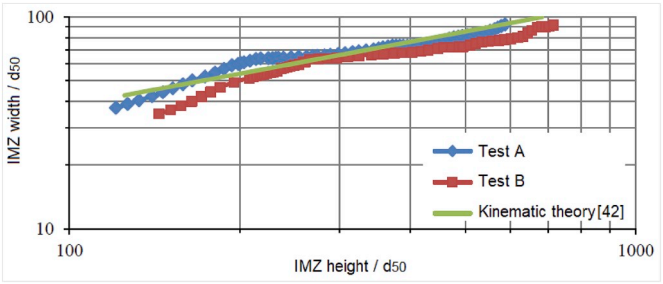

Fig. 7. Isolated movement zone geometry evolution.

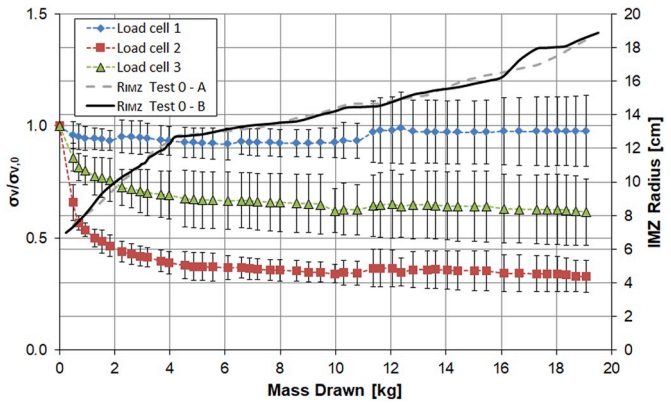

Fig. 8. Induced vertical stress by mass drawn and IMZ radius evolution under mass drawn. Isolated draw. Here, σ_v: vertical stress, $\sigma_{v,0}$: initial vertical stress, R_{IMZ}: IMZ radius (for tests A and B). The error bar shows the vertical stress variability (between tests A and B).

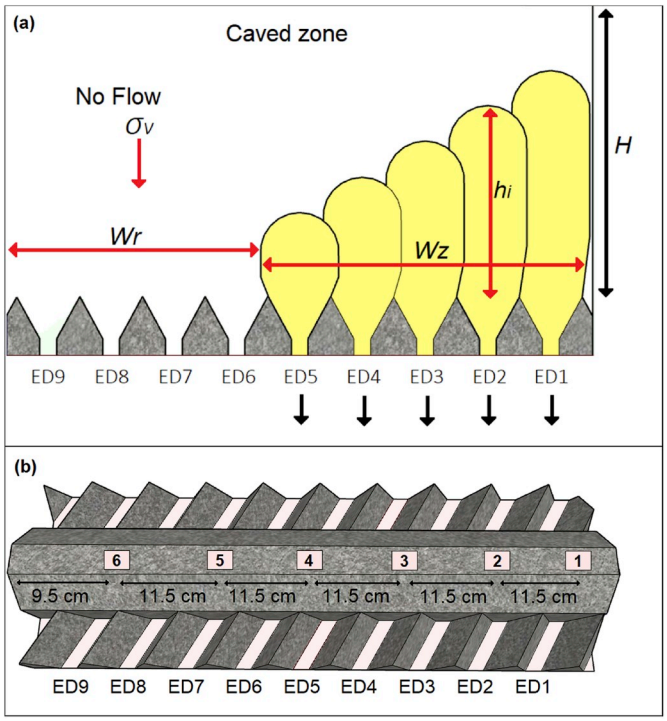

Fig. 9. (a) Panel caving draw strategy configuration (front view) and (b) Load cell location over crown pillar.

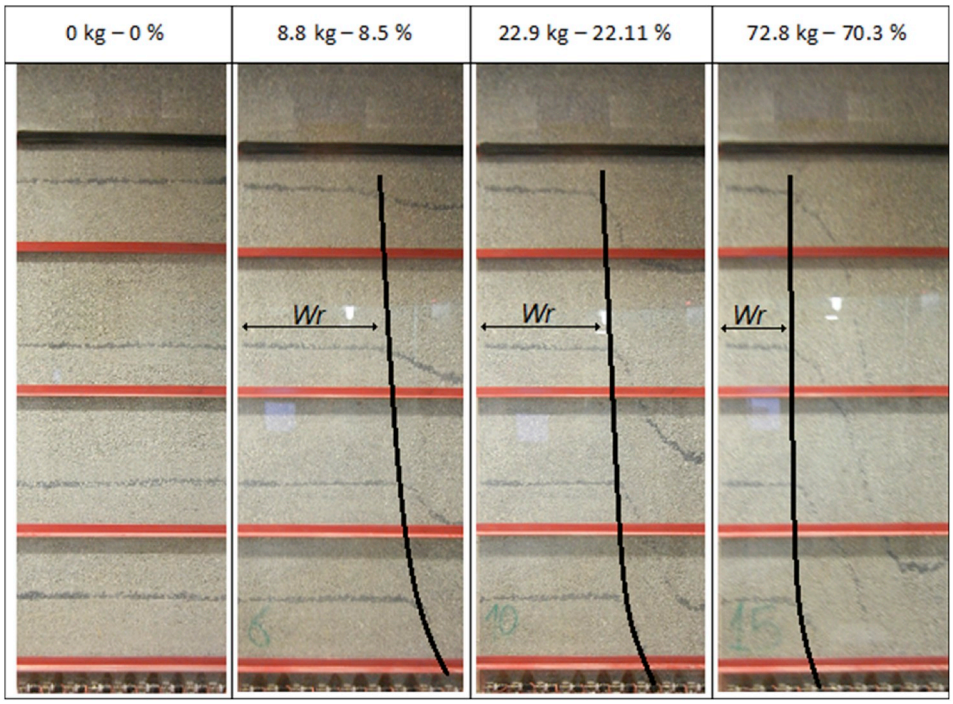

Fig. 10. Test 1 draw evolution during Panel caving draw strategy.

cell 1 (Fig. 11-a) decreased rapidly when extraction started because this cell was below the flow zone, 0.30 $\sigma_{v,0}$. When 40–50 kg of ore was extracted, drawpoints of ED 1 and 2 were closed, this increased the induced vertical stress to 1.36 $\sigma_{v,0}$. Load cell 2 showed similar behaviour with stress variations between 0.26 $\sigma_{v,0}$ below the flow, increasing to 0.54 $\sigma_{v,0}$ when EDs were closed. Load cell 3 was located in the stagnant zone at the beginning of extraction. The vertical stresses showed no change in value until drawpoints near (ED4) were extracted; at which point, induced vertical stress decreased to 0.26 $\sigma_{v,0}$ (Fig. 11-a). Vertical stresses on load cells 4, 5 and 6, located initially in the stagnant zone away from drawpoints under extraction, continuously increased due to

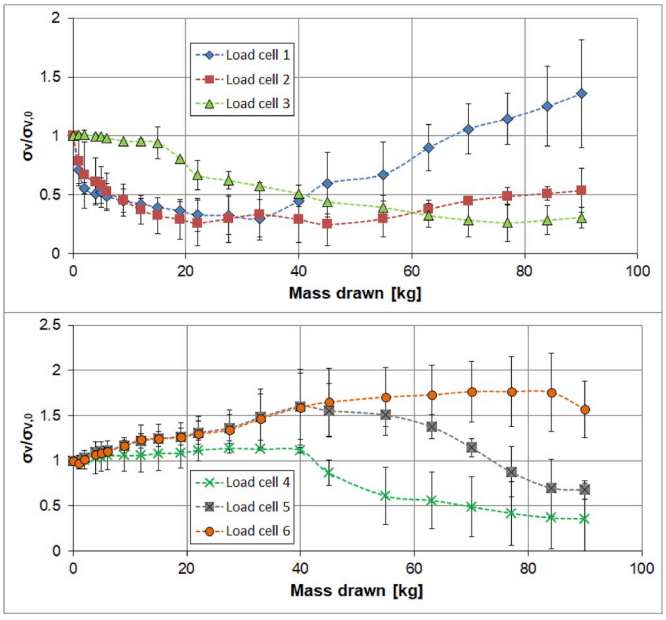

Fig. 11. Induced vertical stresses by mass drawn (a) Results from Load cells 1, 2 and 3 and (b) Results from load cells 4, 5 and 6. Here, σ_v: vertical stress, $\sigma_{v,0}$: initial vertical stress.

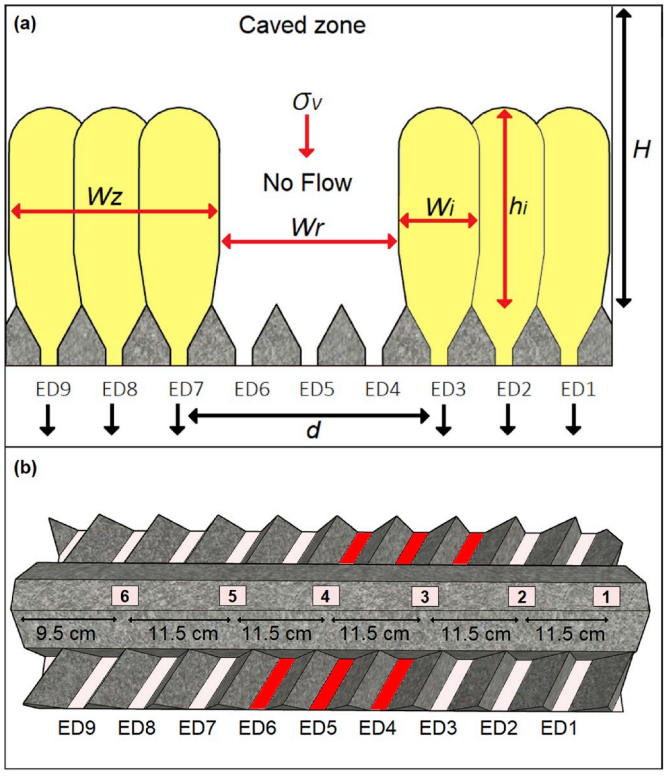

Fig. 12. (a) Block caving draw strategy configuration with high non-draw zone (front view) and (b) Load cell location over crown pillar.

the extraction (Fig. 11-b). In these cells, vertical stresses increased even though the mass in the model was continuously decreasing. Then, vertical stress on load cell 4 decreased to 0.36 $\sigma_{v,0}$ when the load cell was below the flow zone at the end of the test. In this test, load cell 6 reached the maximum value observed of 1.77 $\sigma_{v,0}$.

In the non-draw zone, a direct relation was observed in load cells 4, 5 and 6, between the vertical stress and the stagnant zone width (*Wr*), such that when the stagnant zone decreased, the vertical stress increased.

3.3. Test 2 and 3: block caving draw strategies

In tests 2 and 3, ore was extracted from the drawpoints in the outer areas at the same time. For those drawpoints located in the middle of the model, ore was not extracted until the end of the tests.

3.3.1. Test 2: non-ideal draw with 60 m of unmoved zone

The outer area extraction drifts (EDs) were drawn together while three EDs were not drawn in the middle (see Fig. 12). The flow zone evolution indicates that initially the flow zones interact among EDs 1 and 3 and, separately, among EDs 7 to 9, leaving an unmoved zone, which has a width (*Wr*) observed in Fig. 13.

When extraction progressed, the flow zones of each group of extraction drifts interacted in height, leaving just a small portion of unmoved volume at the ore bottom. After approximately 95 kg extracted, draw strategy changed as EDs under draw (ED 1, 2, 3 and 7, 8, 9) were stopped and drawing was started from ED 4, 5 and 6.

Vertical stress measurements are shown in Fig. 14. The load behaviour observed was as follows:

Load cells 1, 2, 5 and 6 were placed within flow zones. When extraction began, vertical stresses in these cells decreased to 0.31 $\sigma_{v,0}$ and were maintained at that level until draw strategy changed.

For Load cells 3 and 4, located under the stagnant zone (*Wr*), vertical stresses were increased to 1.86 $\sigma_{v,0}$ and 1.51 $\sigma_{v,0,}$ respectively. The difference could have occurred because load cell 4 was closer to a movement zone. Afterwards, as the moving front approached the location of the cells, the load decreased as much as 0.9 times from its original value. At the end of the experiment, when drawing from extraction drifts 4 to 6 started, the vertical stress of these cells decreased 0.36 and 0.39 times from their original value, respectively.

At the end of the experiment (around 95 kg), extraction from the EDs 1 to 3 and 7 to 9 was stopped and EDs 4 to 6 were drawn. A subsequent increase of vertical stresses on these cells was observed, reaching 0.6 to 1.1 of their initial value.

Load cell 3 registered the highest vertical stress on this test. It was placed in the middle of the stagnant zone. In this case, induced vertical stresses increased up to 1.86 $\sigma_{v,0}$ and decreased continuously due to the mass removal from the system. Then, when extraction drifts 4 to 6 were drawn, the induced vertical stress decreased to 0.35 $\sigma_{v,0}$.

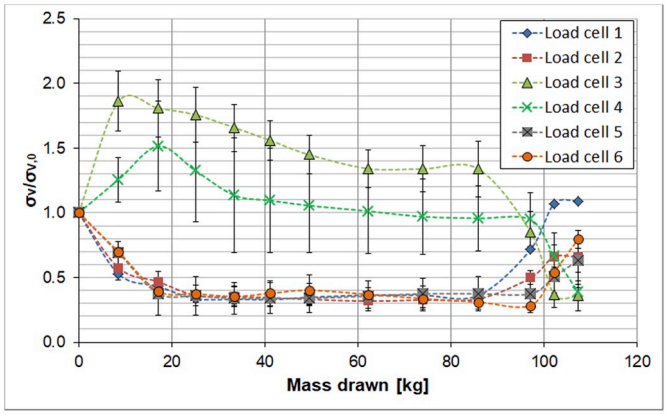

Fig. 14. Induced vertical stresses by mass drawn load cells 1 to 6. Here, σ_v: vertical stress, $\sigma_{v,0}$: initial vertical stress.

3.3.2. Test 3: non-ideal draw with 30 m of unmoved zone

In this test, the same strategy as test 2 was used, but with a minor unmoved zone to quantify higher induced vertical stress, and the relation between the draw and non-draw areas as indicated in theory.[39] Here, only ED5 was not drawn (Fig. 15), while other EDs were under draw. A small pillar was induced with draw strategy. One load cell was located within the non-draw zone (load cell 3 in Fig. 15-b, through ED5 considering the El Teniente layout), while the other four load cells were located in draw zones over the crown pillar.

The evolution of flow zones showed that the no-flow zone rapidly disappeared as flow zones interacted leaving only a small, unmoved zone. In Fig. 16 it can be seen that the flow zones from both draw areas are interacting.

From the measurements of load cells shown in Fig. 17, the vertical stress behaviour was as follows:

Load cell 3 was located in the permanent unmoved zone. In this case the induced vertical stress increased up to 2.81 $\sigma_{v,0}$. After 20 kg of continuous draw, the movement zones overlapped over cell 3. The stress here then decreased but was still higher than at its initial value (see Fig. 17). At the end of the experiment, after 100 kg of extraction, an extraction drift below this cell was opened, and drawing started. In this case, the stress decreased as much as 45% from its original value.

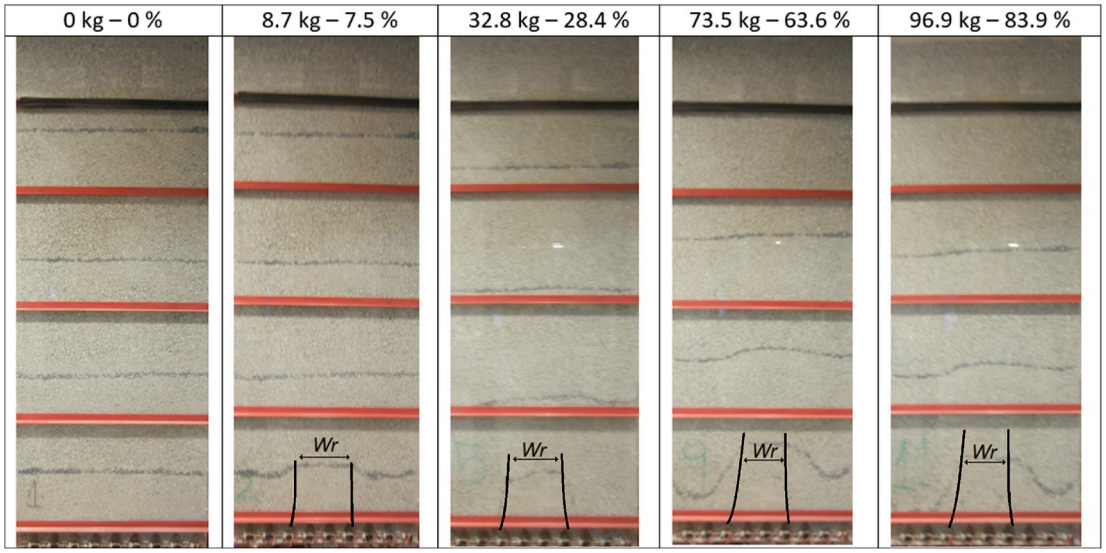

Fig. 13. Test 2 draw evolution in Block caving draw strategy (60 m).

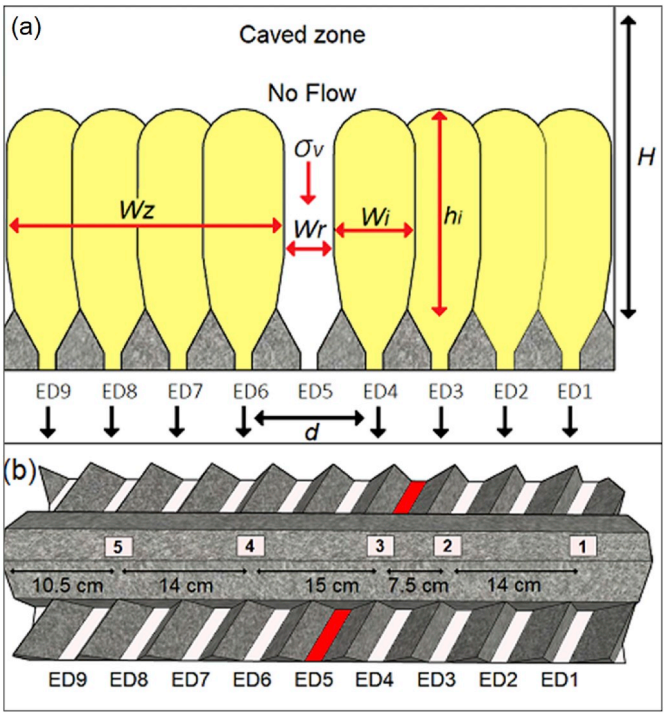

Fig. 15. (a) Block caving draw strategy configuration with high non-draw zone (front view) and (b) Load cell location over crown pillar.

Load cells 1, 2, 4 and 5 were placed below the flow zone and all these cells showed a decrease in their stresses. The induced vertical stress of these cells decreased by around 45% from their original values. When extraction drift 5 was opened, the other extraction drifts were closed, and induced vertical stress in these cells increased from 0.8 to 1.4 $\sigma_{v,0}$.

4. Discussion

This study quantified the effect of key variables on induced vertical stresses in granular material. These variables are the presence of unmoved and moved areas, mass drawn, and distance to the extraction front from any point in the unmoved and moved zones. Although previous studies have suggested a relationship among the variables studied, few physical models have been used to actually measure the effects of these variables on induced stresses on granular material related to draw policies. Our study also took into consideration different draw strategies commonly used in block and panel caving mines.

Fig. 18 shows the induced vertical stress measured in the stagnant zone, σ_V(SZ – exp), and in the movement zone, σ_V(MZ – exp), from Test 1: Panel caving draw strategy. Here, Eq. (6) is used to compare induced stress estimated with vertical stress measured in the movement zone, showing a good correlation with a standard deviation of 2.3. Additionally, the vertical stresses in the movement zone are calculated with the Janssen approach presented in Eq. (1).[21] A good fit is obtained considering k as (1-senφ) and u as 2.6, i.e. vertical stress is higher than horizontal stress on the movement zone of this experiment. In addition, a good fit can also be obtained using Eq. (3). Fig. 18 shows results until 22 kg to avoid variation on stresses due to loss of weight.

To analyse the induced vertical stress in block caving strategies and compare this with the results obtained in panel caving strategies,

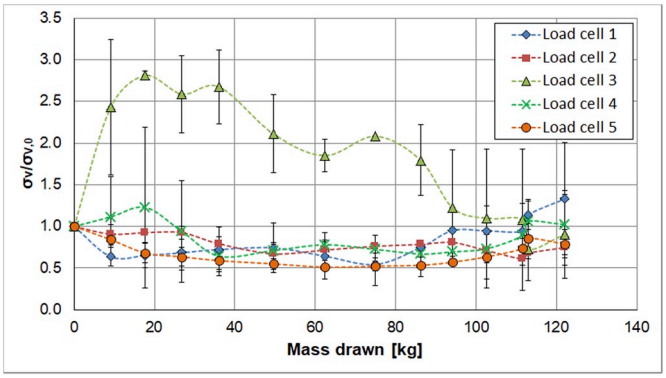

Fig. 17. Induced vertical stresses by mass drawn on load cells 1 to 5. Here, σv: vertical stress, σv,0: initial vertical stress.

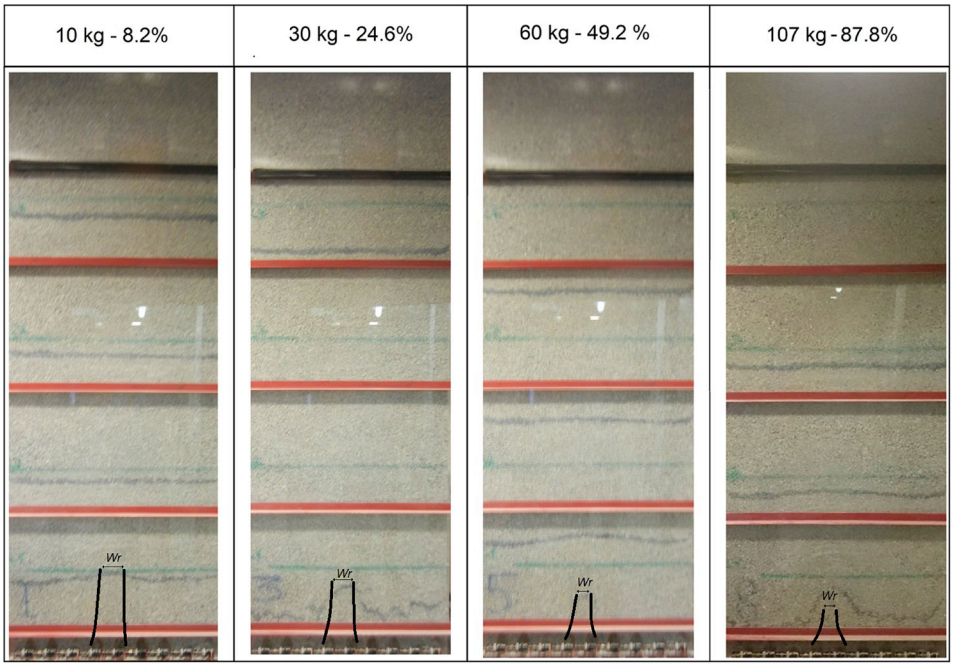

Fig. 16. Test 3 draw evolution in Block caving draw strategy (30 m).

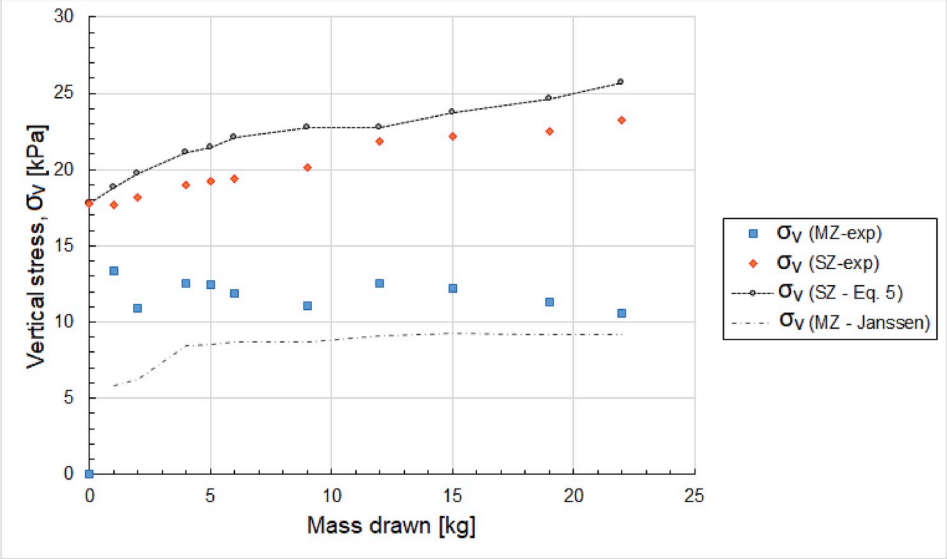

Fig. 18. Induced-vertical stresses in movement and stagnant zones.

induced vertical stress in the stagnant zone, σ_v^{SZ} is calculated rewriting Eq. (6) and normalizing it by the initial vertical stress, σ_{v0} as,

$$\frac{\sigma_v^{SZ}}{\sigma_{v0}} = \left(A_T - \frac{\sum \sigma_v^{MZ} A_{MZ}}{\sigma_{v0}}\right) \frac{1}{A_{sz}} \tag{7}$$

Where σ_{v0} is the initial vertical stress, A_T is the total caved area, σ_v^{MZ} is the vertical stress in the movement zone, A_{MZ} is the area of the movement zone and A_{sz} is the area of the stagnant zone. It should be noted that the induced vertical stress in the stagnant zone increases when the area of the stagnant zone decreases. Additionally, in the stagnant zone the induced vertical stress depends on the vertical stress in the movement zone. This relation between the induced vertical stress in the stagnant zone and its area is shown in the draw test in Fig. 19.

Fig. 19 shows the vertical stress measured in the stagnant zone in Test 1, 2 and 3, and the induced vertical stress calculated using Eq. (7), which used vertical stress measured in the movement zone of tests. As observed previously in Fig. 18, induced stress correlates well with the panel caving strategy in Fig. 19. However, in block caving tests, Eq. (7) overestimates the induced vertical stress. The overestimation of induced stress may occur because when both movement zones are in contact, the stress related to the initial density of the material is decreased in the stagnant zone.

The results obtained from this experimental set up can be used to define extraction policies to alleviate induced vertical stresses within caved materials. Based on our results, one such strategy would be to increase the unmoved area proximal to drawpoints to allow vertical stress to act on a larger area. Another strategy would be to draw from unmoved zones to decrease stress.

Many other interesting variables were not included in our study whose main objective was to quantify induced stress due to ore draw under controlled conditions. It would be useful in future studies to observe the effects of variables such as humidity, draw rates and uniformity of draw on induced stress. Furthermore, findings from this study suggest other related studies. For example, future set ups could be constructed to more deeply analyse production pillar stability and the influence of shear zones during ore draw.

5. Conclusions

In the flow zones of the different draw strategies, lower vertical stresses were measured, and consequently, as expected, there were higher vertical stresses under no-flow zones. The size of the unmoved or moved areas influenced the magnitude of the induced vertical stresses.

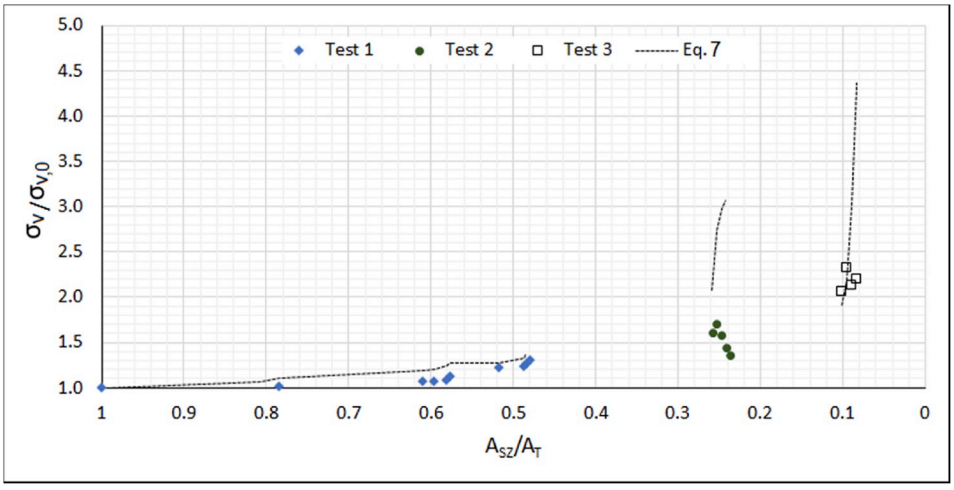

Fig. 19. Induced-vertical stresses over stagnant zone relative to total area.

While the unmoved zone width decreased, the vertical stresses increased here, and this was observed both in block caving and panel caving draw strategies.

In block caving strategies, it was found that vertical stress could increase between 2 and 3 times its initial value when different unmoved zone widths were tested. On the other hand, with regard to panel caving, the maximum vertical stress measured was found to be a function of the distance to the front of the draw zone and could reach values close to 2 times initial values. Knowing these magnitudes, not only can extraction policies be used to alleviate induced stress but also the maximum stress that can be expected on the production-level pillars can be estimated in the beginning stages of a project. Then, support systems could be designed according to these requirements, thus avoiding problems like those described by Sahupala et al., [17] Bravo, [18] Pierce, [20] and most likely in various other unpublished cases.

Declaration of competing interest

Authors declare that we don't have conflict of interest and all de funding sources have been included.

Acknowledgment

This paper was (partially) funded by the CONICYT/PIA Project AFB180004. The authors gratefully acknowledge the support of the Block Caving Laboratory and the Advanced Mining Technology Centre of the University of Chile. R. Gómez acknowledges the support of CONICYT PFCHA/DOCTORADO BECAS CHILE/2018 – 21180046.

References

1 Flores G. Future challenges and why cave mining must change. In: *3rd International Symposium on Block and Sublevel Caving. Santiago, Chile*. June 2014:23–52, 5-6.
2 Fairhurst C. Some challenges of deep mining. *Engineering*. 2017;3(4):527–537.
3 Laubscher DH. Cave mining-the state of the art. *J S Afr Inst Min Metall*. 1994;94(10):279–293.
4 Trueman R, Pierce M, Wattimena R. *Quantifying Stresses and Support Requirements in the Undercut and Production Level Drifts of Block and Panel Caving Mines*. Minneapolis, USA: JKMRC, The University of Queensland, Australia. Itasca Consulting Group; 2002.
5 Brown ET. Cave initation by undercutting. In: *Block Caving Geomechanics, 2nd Edition, the International Caving Study 1997 – 2004, JKMRC*. The University of Queensland; 2007:229–287.
6 Bartlett PJ, Croll A. Cave mining at premier mine. In: *Massmin 2000 Proceedings. Brisbane, Australia; 29 October – 2*. November 2000:227–234.
7 Callahan MF, Keskimaki KW, Fronapfel LC. Constructing and operating Henderson's new 7210 production level. In: *Massmin 2008, 5th International Conference & Exhibition on Mass Mining. Lulea, Sweden; 9-11*. June 2008:15–24.
8 Araneda O, Sougarret A. Lessons learned in cave mining at the El Teniente mine over the period 1997-2007. In: *Massmin 2008, 5th International Conference & Exhibition on Mass Mining. Lulea, Sweden; 9-11*. June 2008:43–52.
9 Fernandez F, Evans P, Gelson R. Design and implementation of a damage assessment system at Argyle Diamond's block cave project. In: *Caving 2010, Proceeding of the Second International Symposium on Block and Sublevel Caving. Perth, Australia; 20-22*. April 2010:65–81.
10 Lett JL, Brunton I, Capes GW, et al. Undercutting to surface breakthrough – Cadia East panel cave (stage 1). In: *Seventh International Conference & Exhibition on Mass Mining, Proceeding. Sydney, Australia; 9-11*. May 2016:65–82.
11 Snyman L, Webster S, Samosir J. E48 cave extension at Northparkes. In: *Seventh International Conference & Exhibition on Mass Mining, Proceeding. Sydney, Australia; 9-11*. May 2016, 111-17.
12 Rojas E, Molina R, Bonani A, Constanzo H. The pre-undercut caving method at the El Teniente mine, Codelco Chile. In: *Massmin 2000 Proceedings. Brisbane, Australia; 29 October – 2*. November 2000:261–266.
13 Quiñones L, Lagos C, Ortiz F, Farías E, Toro L, Villegas D. Undercut advance direction management at the North 3rd panel, Rio Blanco mine, División Andina Codelco Chile. In: *3rd International Symposium on Block and Sublevel Caving. Santiago, Chile; 5-6*. June 2014:91–97.
14 Viegas G, Bosman K, Angus D, De Beer W, Urbancic T. Mapping cave front growth utilising the collective behaviour of seismicity and velocity fields. In: *Caving 2018, Fourth International Symposium on Block and Sublevel Caving. Vancouver, Canada; 15-17*. October 2018, 577-88.
15 Shen WL, Bai JB, Wang XY, Yu Y. Response and control technology for entry loaded by mining abutment stress of a thick hard roof. *Int J Rock Mech Min Sci*. 2016;100(90):26–34.
16 Richardson MP. Area of draw influence and drawpoint spacing for block caving mines. In: DR Stewart DR, ed. *Design and Operation of Caving and Sublevel Stoping Mines*. 1981:149–156. New York.
17 Sahupala H, Brannon C, Annavarapu S, Osborne K. Recovery of extraction pillars in the deep ore zone (DOZ) block cave, PT freeport Indonesia. In: *Massmin 2008, 5th International Conference & Exhibition on Mass Mining. Lulea, Sweden; 9-11*. June 2008, 191-02.
18 Bravo C. *Recuperación de reservas colapsadas en minas panel caving. Bachelor degree*. Santiago: Universidad de Chile; 2010 (in Spanish).
19 Orellana M, Cifuentes C, Díaz J. Caving experiences in Esmeralda sector, El Teniente mine. In: *3rd International Symposium on Block and Sublevel Caving. Santiago, Chile; 5-6*. June 2014:78–90.
20 Pierce ME. Forecasting vulnerability of deep extraction level excavations to draw-induced cave loads. *Journal of Rock Mechanics and Geotechnical Engineering*. 2019;11(3):527–534.
21 Janssen HA. Experiments regarding grain stress in soils. *Zeitschrift Des Vereines Deutscher Ingeniure*. 1985;39(35):1045–1049. Translated from German by W. Hustrulid and N. Krauland in Proceedings of the Massmin 2004. Santiago, Chile. p. 293-00.
22 Walker D. An approximate theory for pressures and arches in hoppers. *Chem Eng Sci*. 1966;21:975–997.
23 Jenike AW, Johanson JR, Carson JW. Bin loads—Part 3: mass-flow bins. *J Eng Ind*. 1973;95(1):6–12.
24 Jaky J. Earth pressure – pressure in silos. In: *Proceeding of the Second International Conference on Soil Mechanics and Foundation Engineering. Rotterdam; 21-30*. june 1948:103–107.
25 Pieper K. Investigation of silo loads in measuring models. *J Eng Ind*. 1969;91(2):365–372.
26 Nedderman RM. The method of differencial slices. In: *Statics and Kinematics of Granular Materials*. Cambridge: University Press; 1992, 84-26.
27 Hoeg K. Stresses against underground structural cylinders. *J Soil Mech Found Div*. 1968;94:833–858.
28 Deutsch GP, Schmidt LC. Stresses on silo walls. *J Eng Ind*. 1969;91(2):450–457.
29 Munch-Andersen J, Ditlevsen O, Christensen C, Randrup-Thomsen S, Hoffmeyer P. Empirical stochastic silo load model. II: data Analysis. *J Eng Mech*. 1995;121(9):981–986.
30 Vanel L, Claudin P, Bouchaud JP, Cates ME, Clément E, Wittmer JP. Stresses in silos: comparison between theoretical models and new experiments. *Phys Rev Lett*. 2000;84(7):1439.
31 Chou CS, Chuang YC, Smid J, Hsiau SS, Kuo JT. Flow patterns and stresses on the wall in a moving granular bed with eccentric discharge. *Adv Powder Technol*. 2002;13(1):1–24.
32 Berntsen KN, Ditlevsen OD. Stochastic stresses in granular matter simulated by dripping identical ellipses into plane silo. In: *8th International Conference on Applications of Probability and Statistics to Civil Engineering*. 2000:57–64.
33 Colonnello C, Reyes LI, Clément E, Gutiérrez G. Behavior of grains in contact with the wall of a silo during the initial instants of a discharge-driven collapse. *Phys Stat Mech Appl*. 2014;398:35–42.
34 Kobyłka R, Horabik J, Molenda M. Numerical simulation of the dynamic response due to discharge initiation of the grain silo. *Int J Solid Struct*. 2017;106:27–37.
35 Castro R. *Study of the Mechanisms of Gravity Flow for Block Caving*. PhD thesis. Australia: The University of Queensland; 2006.
36 Orellana LF. *Evaluación de variables de diseño del sistema de minería continua a partir de experimentación en laboratorio*. MSc. Thesis. Santiago: Universidad de Chile; 2012 (in Spanish).
37 Vergara P. *Estudio experimental de flujo gravitacional en minería de panel caving*. Bachelor degree. Santiago: Universidad de Chile; 2016.
38 Lorig LJ. *Relation between Caved Column Height and Vertical Stress at the Cave Base*. Final Report. International Caving Study, JKMRC and Itasca Consulting Group, Inc.; 2000.
39 Pierce M. *A Model for Gravity Flow of Fragmented Rock in Block Caving Mines*. PhD Thesis. Australia: The University of Queensland; 2009.
40 Knappett JA, Craig RF. Basic characteristics of soils. In: *Carig's Soil Mechanics*. eighth ed. Spon press editorial; 2012:3–38.
41 Cho G, Dodds D, Santamarina JC. Particle shape effects on packing density, stiffness, and strength: natural and crushed sands. *J Geotech Geoenviron Eng*. 2006;16(5):451–471.
42 Nedderman RM. The use of the kinematic model to predict the development of the stagnant zone boundary in the batch discharge of a bunker. *Chem Eng Sci*. 1995;50(6):959–965.